Annals of Glaciology



Article

Cite this article: Alemany O et al. (2021). The SUBGLACIOR drilling probe: hydraulic considerations. *Annals of Glaciology* **62**(84), 131–142. https://doi.org/10.1017/aog.2020.79

Received: 25 June 2020
Revised: 20 October 2020
Accepted: 21 October 2020
First published online: 27 November 2020

Key words:
Glaciological instruments and methods; ice coring; ice engineering; paleoclimate

Author for correspondence:
Olivier Alemany,
E-mail: olivier.alemany@univ-grenoble-alpes.fr

© The Author(s), 2020. Published by Cambridge University Press. This is an Open Access article, distributed under the terms of the Creative Commons Attribution licence (http://creativecommons.org/licenses/by/4.0/), which permits unrestricted re-use, distribution, and reproduction in any medium, provided the original work is properly cited.

cambridge.org/aog

The SUBGLACIOR drilling probe: hydraulic considerations

O. Alemany[1,2], P. Talalay[3], P. Boissonneau[1,2], J. Chappellaz[1,2], J. F. Chemin[1,2], R. Duphil[1,2], E. Lefebvre[1,2], L. Piard[1,2], P. Possenti[1,2] and J. Triest[1,2]

[1]CNRS, IGE, F-38000 Grenoble, France; [2]LGGE, Université Grenoble Alpes, F-38000 Grenoble, France and [3]Polar Research Center, Jilin University, Changchun 130021, China

Abstract

Using significant technological breakthroughs and unconventional approaches, the goal of the in situ probing of glacier ice for a better understanding of the orbital response of climate (SUBGLACIOR) project is to advance ice core research by inventing, constructing and testing an in situ probe to evaluate if a target site is suitable for recovering ice as old as 1.5 million years. Embedding a laser spectrometer, the probe is intended to make its own way down into the ice and to measure, in real time and down to the bedrock, the depth profiles of the ice δD water isotopes as well as the trapped CH_4 gas concentration and dust concentration. The probe descent is achieved through electromechanical drilling combined with continuous meltwater sample production using a central melting finger in the drill head. A key aspect of the project lies in the design and implementation of an efficient method to continuously transfer to the surface the ice chips being produced by the drill head and from the refreezed water expulsed downstream from the melting finger, into the borehole. This paper presents a detailed calculation and analysis of the flow rates and pressure conditions required to overcome friction losses of the drilling fluid and to effectively transport ice chips to the surface.

1. Introduction

Within the framework of the in situ probing of glacier ice for a better understanding of the orbital response of climate (SUBGLACIOR) project (Alemany and others, 2014), a laser spectrometer is mounted inside an ice drilling probe, in order to obtain fundamental climatic signals (water isotopic ratios, CH_4 concentration in trapped gas as well as dust concentration) while drilling the Antarctic ice sheet, with real time data production and transfer towards the surface. The probe is linked to the surface with an electromechanical cable (enabling the transmission of data and power to/from the probe) and with a hosepipe (to transport clean drilling fluid from the surface to the drill head). The probe, cable and hosepipe are connected in the uppermost part of the probe. A mechanical drill head (at the tip of the probe) cuts the ice over 98% of the surface of the borehole, while the remaining 2% are melted with a melt finger centred in the drill head and extending down by 25 cm.

The chips produced while electromechanically cutting the ice are carried by the drilling fluid flow through the free space between the probe and the borehole wall and then into the annulus space between the borehole wall and the hosepipe. The source of the drilling fluid flow lies in a hydraulic pump located at the surface.

Upon reaching the surface, the chips are separated from the drilling fluid by an industrial separation device. After cleaning, the drilling fluid is re-injected into the borehole through the hosepipe, while the ice chips are stored at the surface (Fig. 1). Because the ice chips must be recovered at the surface to avoid borehole clogging, it is mandatory to bring the fluid level up to the surface. This requires installing a leak-tight casing throughout the firn column. This type of casing has already been tested at Concordia Station, Antarctica (Duphil and others, 2014) with modest success.

The melt finger located under the electromechanical drill head melts 2% of the bottom surface of the ice (Fig. 2). The produced meltwater is pumped into the probe and carried through a sample handling line, where the gas phase (dissolved in the water under ambient pressure) is separated from the water phase at atmospheric pressure through a debubbler and then analysed by the built-in laser spectrometer. The degassed meltwater is then pressurised with an embedded high-pressure pump, injecting water droplets in the annulus section between the probe and the walls of the borehole. The water droplets immediately freeze and are transformed into ice chips mixed with those produced from the electromechanical drill head.

The SUBGLACIOR fluid circulation principle bears some resemblance to rock drilling by oil companies (e.g. Nguyen, 1993). However, the nature and temperature of the drilling fluid, the drilling fluid flow rate, the nature of the cuttings, the weight on the bit, and the head rotation speed are different. Thus, hydraulic calculations used to dimension oil drilling systems could not be directly applied to the SUBGLACIOR context.

Once our design included a high-pressure hydraulic pump located at the surface to circulate the drilling fluid up the borehole while carrying the ice chips from the drilling head up to the surface, the following points had to be addressed:

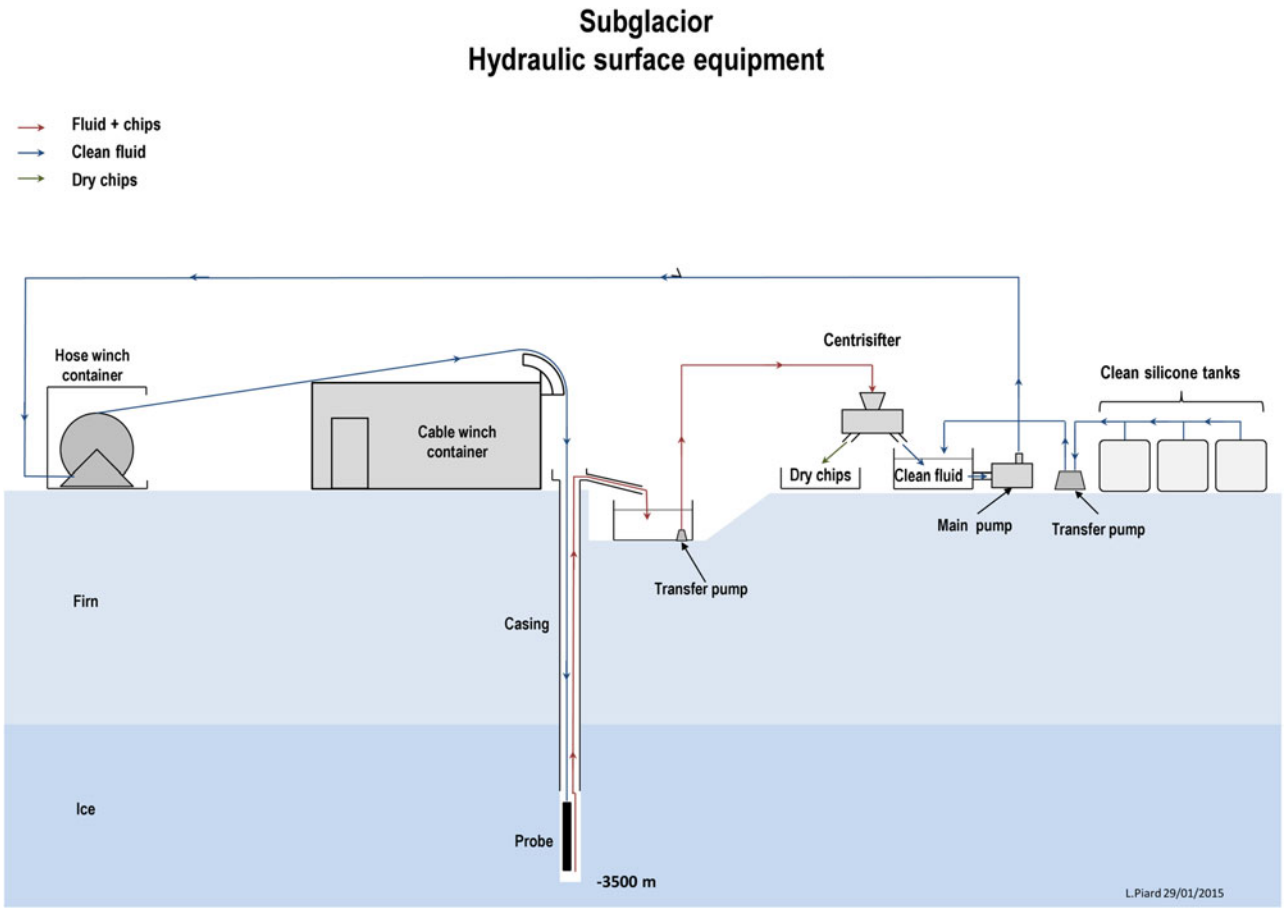


Fig. 1. Schematic of the SUBGLACIOR hydraulic circulation principle.

- Which drilling fluid should be used?
- Is there a minimum fluid velocity required to move the ice chips upward?
- What are the pump requirements to generate sufficient fluid flow in order to move the ice chips upward?

2. Drilling fluid

Deep boreholes in the ice require to be filled with a fluid in order to compensate for the ice pressure (Talalay and Gundestrup, 2002*a*). Selecting a new drilling fluid that can be used at very low temperatures (down to −55 °C) in the conditions of the Antarctic plateau is a major question that the whole ice drilling community currently faces, since it is no longer possible to use the drilling fluid densifier HCFC 141b in Antarctica. During the SUBGLACIOR pre-design period, we carried out bibliographic research (Talalay and Gundestrup, 2002*b*), investigations, and tests on various alternative drilling fluids (Triest and Alemany, 2014). The best compromise for the SUBGLACIOR project between the drilling requirements and the risk of artefacts in the spectrometer measurements is silicone oil with a viscosity of 3 $mm^2 s^{-1}$ (or 3 cSt).

The density of silicone oil can counterbalance the ice pressure (930 $kg m^{-3}$ at 0 °C and 970 $kg m^{-3}$ at −40 °C); its freezing point is ∼−120 °C and its kinetic viscosity is low (3 $mm^2 s^{-1}$ at 25 °C) even if it increases rapidly below this rate at low temperatures (13 $mm^2 s^{-1}$ at −40 °C, which is three times higher than the usual drilling fluid mixture made of kerosene and HCFC 141b). Furthermore, this fluid is environmentally friendly and does not pollute the spectrometer measurement in case the water sample includes a tiny portion of drilling fluid.

Nevertheless, this fluid has several drawbacks. It is more expensive than Estisol drilling fluids (several €/kg) and it has a very low surface tension (∼20 $mN m^{-1}$, which is less than water at 20 °C ≈ 73 $mN m^{-1}$). The low surface tension can be problematic when the fluid is used in conjunction with plastic impeller pumps. If silicone oil moves between the impeller and the casing (with very low pressure and very high speed), it can create cavitation and it can lead to impeller destruction within a few hours.

Tests have been conducted on three different silicone oil types (described in the next section). The three of them were convenient, and it is for the economical reason that we choose BlueStar 47V3 oil for the SUBGLACIOR project.

3. Ice chip behaviour in silicone oil

Tests were carried out in cold rooms at temperatures between −5 °C and −30 °C to check the behaviour of ice chips in BlueStar 47V3 3 cSt silicone oil (density: 880 $kg m^{-3}$ at 25 °C, 923 $kg m^{-3}$ at −20 °C and 942 $kg m^{-3}$ at −40 °C), Shin-Etsu KF96 2 cSt silicone oil (density: 870 $kg m^{-3}$ at 25 °C and 936 $kg m^{-3}$ at −40 °C) and Momentive BM3 (density: 900 $kg m^{-3}$ at 25 °C, 925 $kg m^{-3}$ at −20 °C). Half a litre of chips, produced by machining a block of artificial ice with a lathe in a cold room, were dropped in a 5 L bowl filled with silicone oil (one bowl with KF96-2 and another one with 47V3).

At the start of the experiment with KF96-2, we could observe that the ice chips tend to float in the fluid (at this temperature, between −5 °C and −10 °C, the ice chip density is just slightly higher than the fluid density). But after a few hours, the ice particles started to sink towards the bottom of the bowl. After 2 days,

https://doi.org/10.1017/aog.2020.79 Published online by Cambridge University Press



Fig. 2. The heating element at the tip of the probe.

all the particles lied at the bottom of the bowl. This mixture was then left to rest in the cold room. After 6 weeks, it was agitated with a stirrer. The ice chips fully mixed again with the drilling fluid, without any tendency for agglomeration.

The same experiment was conducted with a bowl containing 47V3 and BM3 silicone oil. Both oils have very similar density range and provide nearly the same results.

At −10 °C, the ice density is slightly higher than the density of the ice chips. Some ice chips sink and others stay at the surface of the bowl. After 3 days, all the chips were finally laying at the bottom of the bowl.

At −20 °C, when the oil density is in the same range of values as the ice density, we noticed that after 24 h, some ice chips sink and stay in the middle of the bowl (mid-depth) and others stay at the surface. After 3 days, all the ice particles were at the top of the bowl.

At −30 °C, all the ice chips stay at the surface after 3 h of testing. Here again, after 2 weeks of testing, and in any temperature situation, we did not observe any hard conglomeration.

Thus, it appears that ice chips do not conglomerate in silicone oil. It is very likely that the silicone oil covers the ice chips with a thin oil coating that prevents any particle agglomeration.

4. Surface pump requirement

The surface pump requirement (flow rate, pressure) depends on the pressure loss calculation along with the drilling fluid circulation system. Drilling fluid is injected into the hosepipe using a pump at the surface. The fluid is pumped down the hose to the drilling probe, and then it is transferred through the probe itself using channels to drill head. Once the fluid reaches the drill head, it continuously picks up the ice chips generated while drilling and carries them up to the surface.

In order to determine optimal hydraulic working conditions, pressure losses were calculated along a flowline from the surface to the probe and then back to the surface. Once the pressure losses are known, it is possible to determine the pump requirement needed to compensate for these losses.

The required flow rate of the drilling fluid Q ($m^3\,s^{-1}$) of the pump is calculated according to the following equation:

$$Q = \frac{\pi}{4C_{\max}}(D^2 - d_2^2)\mathrm{ROP}, \tag{1}$$

where D is the outer diameter (OD) of the drill head and d_2 is the diameter of the hosepipe, m; ROP is the expected rate of penetration, $m\,s^{-1}$; and $C_{\max}$ is the maximum concentration of the cuttings in the fluid (to avoid packing $C_{\max}$ is set at ≤5% of the concentration according to Talalay, 2006).

The outlet pressure p_p (Pa) of the pump should not be less than the head losses in the circulation system, following the equation:

$$p_p = k_s(\sum p_f + \sum p_l), \tag{2}$$

where k_s is the safety coefficient (in conventional rock drilling $k_s = 1.3$–1.5); p_f is the pressure losses due to hydraulic resistances (due to the friction) at various parts of the circulation system, Pa; p_l is the local pressure losses resulting from rapid changes in the direction or magnitude of the fluid velocity at entrances, bends, changes of diameter or effective area and other similar modifications of the circulation system.

Local pressure losses (Pa) are usually expressed in terms of the local loss coefficient k_l, which depends on the geometry of the circulation system according to

$$p_l = k_l \frac{\rho_f U^2}{2}. \tag{3}$$

where ρ_f is the fluid density, $kg\,m^{-3}$, and U is the mean fluid velocity, $m\,s^{-1}$.

For a long uniform straight hosepipe, the local pressure losses are much smaller than the friction losses. With a flow rate in the range of 30–40 $L\,min^{-1}$ and with a hosepipe having an inner diameter (ID) of 31.75 mm (1.25 in), the maximum fluid velocity will be in-between 0.6 and 0.8 $m\,s^{-1}$. Even if the exact geometry of the fluid loop in the probe itself is difficult to model precisely, as a first approximation we considered <20 abrupt changes of diameter or effective area, 20 sharp bends, 20 valves, and 20 exits and abrupt expansions. In this configuration, the total local pressure losses are <0.05 MPa (Belvins, 1984).

Friction pressure losses depend on the length of the flowline, which is 3500 m long in the case of SUBGLACIOR, on the fluid characteristics (viscosity, density, Reynolds number) and on the roughness of the hosepipe. Along the first section of the hydraulic line (from the surface – Point 1 – down to the probe – Point 2, Fig. 1), the friction losses are calculated with a clean drilling fluid. In the second section of the hydraulic line (from the drill head – Point 2 – to the surface – Point 3, Fig. 1), the friction losses are calculated for a drilling fluid mixed with 5% of ice chips in volume. The mean viscosity and mean density of this mixture were calculated taking the particle concentration into account (Alemany and Mityar, 2007).

Friction pressure losses can be calculated using the Darcy–Weisbach equation

$$p_f = \lambda_r \frac{L}{D_h}\frac{\rho_f U^2}{2}, \tag{4}$$

https://doi.org/10.1017/aog.2020.79 Published online by Cambridge University Press

Table 1. Pump requirement for a 1.25 in hosepipe

C_{max}, %	Q, L min^{-1}	U_1, m s^{-1}	Re_1	λ_1	p_1, MPa	U_2, m s^{-1}	Re_2	λ_2	p_2, MPa	p_p, MPa	N_p, kW
2	49.2	1.035	3072	0.0425	2.363	0,084	272	0.2353	0.088	3.251	6.66
3	32.8	0.690	2048	0.0470	1.162	0,056	181	0.3530	0.058	1.652	2.26
4	24.6	0.518	1536	0.0417	0.579	0,042	136	0.4706	0.044	0.875	0.90
5	19.7	0.414	1229	0.0521	0.463	0,033	109	0.5883	0.035	0.713	0.58

where L is the total length of the circulation line, m; D_h is the hydraulic diameter, m (for downward flow, it is equal to the ID of the hosepipe d_1; for the annulus $D_h = D - d_2$, where d_2 is the OD of the hosepipe for upward flow); and λ_r is the roughness coefficient.

In the case of a laminar flow, λ_r does not dependent on the roughness but it varies with the Reynolds number Re, i.e. with the relative strength of the viscous and inertial forces

$$Re = \frac{UD_h}{\nu}, \tag{5}$$

where ν is the kinematic viscosity of the drilling fluid, m^2 s^{-1}.

When Re is <2000 (Comolet, 2006)

$$\lambda_r = \frac{64}{Re}. \tag{6}$$

For Reynolds numbers between 2000 and 4000, the flow changes from laminar to turbulent. Values of λ_r are uncertain in this range. A safe procedure consists of estimates that the flow is turbulent (Brater and others, 1996). When flow occurs at Reynolds numbers >4000, values of λ_r in the Darcy–Weisbach formula vary with roughness as well as with viscosity and density, and the friction factor is more difficult to assess since radial components of velocity exist and there is an interchange of momentum between adjacent layers of the fluid. Turbulent flow may be divided into three categories: flow in smooth pipes, flow in rough pipes at high velocities and flow in the transition zone between the first two categories. In our case, as the surface roughness does not protrude beyond the laminar sub-layer of the boundary flow and at turbulent flow, the roughness coefficient closely approaches:

$$\lambda_r = 0.3164\, Re^{-0.25}. \tag{7}$$

Finally, the shaft power of the driving pump motor can be estimated according to 'N_p':

$$N_p = \frac{p_p Q}{\eta_p}. \tag{8}$$

where η_p is the pump efficiency.

The pump requirement calculations as a function of the maximum concentration of the ice chips in the fluid and flow rate at ROP = 1.5 mm s^{-1} are presented in Tables 1 and 2. The corresponding power requirement is calculated using a pump efficiency of 40%. These calculations were conducted for two hosepipe diameters, one with an ID of 1.25 in and another one with an ID of 1.5 in. The physical properties of the clean fluid and mixture with ice chips are considered for the case of an average temperature in the borehole of −32 °C ($\rho_f = 941$ kg m^{-3}, $\rho_{ice} = 920$ kg m^{-3}, $\nu = 1.07 \times 10^{-5}$ m^2 s^{-1} and $\nu_{f+ice} = 2.34 \times 10^{-5}$ m^2 s^{-1}). Symbols with subscript '1' ('2') refer to the downward (upward) flow, respectively.

The results from these calculations drove our choice of the hose diameter. In terms of pump power consumption, it is better to use the 1.5 in ID hosepipe. For the same fluid flow rate, the gain is significant: the required power is 6.66 kW for a 49.2 L min^{-1} flow rate with a 1.25 in hosepipe, whereas the pump requirement is reduced to 3.05 kW for the same flow rate with a 1.5 in hosepipe.

However, it is not possible to fit a 1.5 in hosepipe on a winch embedded in a 20-foot long high cube container. A 40-foot container would be required for this size of hosepipe, which is not compatible with the available logistics. Therefore, despite the gain in hydraulic loss between 1.25 in and 1.5 in, we chose a 1.25 in hosepipe.

Several pump producers were contacted to provide a pump able to handle a sufficient pressure drop with a flow rate between 25 and 40 L min^{-1}, and being compatible with silicone oil at temperatures <−30/−40 °C. The best pump appeared to be a multicellular side-channel centrifugal pump, with magnetic coupling (GROSCLAUDE ZS-SEMA). This pump can provide a 30 L min^{-1} flow rate under a pressure gradient of 2.5 MPa.

5. Influence of temperature on drilling fluid hydraulics

In reality, the density and viscosity of the drilling fluid change with depth due to temperature variations in the borehole. In addition, the drilling fluid temperature in the downward flow inside the hosepipe varies as a result of heat exchange with the counterflow occurring in the annular space, in which temperature varies through time and with depth due to heat exchange with the surrounding ice. The change in drilling fluid temperature is also associated with the cooling of the drill head and the generation of heat due to the hydraulic friction of the drilling fluid.

Mikhailova (1985) suggested calculating the temperature of the drilling fluid according to

$$t_1 = m_1 e^{r_1 h} + n_1 e^{r_2 h} - a + b + t_0 + \sigma h, \text{ in the downward flow} \tag{9}$$

and

$$t_2 = m_2 e^{r_1 h} + n_2 e^{r_2 h} + b + t_0 + \sigma h, \text{ in the upward flow,} \tag{10}$$

where m_1, m_2, n_1, n_2, r_1, r_2, a and b are estimated coefficients; h is the evolving depth of the borehole during drilling, m; t_0 is the temperature at the depth of zero annual amplitude, °C; and σ is the temperature gradient, °C m^{-1}.

The estimated coefficients are calculated using the following equations:

$$m_1 = -\frac{(t_i - t_0 + a - b) r_2 e^{r_2 H} + (k\pi/Gc)(a - \Delta t_N)}{r_1 e^{r_1 H} - r_2 e^{r_2 H}}; \tag{11}$$

$$n_1 = \frac{(t_i - t_0 + a - b) r_1 e^{r_1 H} + (k\pi/Gc)(a - \Delta t_N)}{r_1 e^{r_1 H} - r_2 e^{r_2 H}}; \tag{12}$$

https://doi.org/10.1017/aog.2020.79 Published online by Cambridge University Press

Table 2. Pump requirement for a 1.5 in hosepipe

C_{max}, %	Q, L min^{-1}	U_1, m s^{-1}	Re_1	λ_1	p_1, MPa	U_2, m s^{-1}	Re_2	λ_2	p_2, MPa	p_p, MPa	N_p, kW
2	49.2	0.719	2560	0.0445	0.994	0.088	262	0.244	0.101	1.487	3.05
3	32.8	0.479	1707	0.0375	0.372	0.058	175	0.366	0.067	0.636	0.87
4	24.6	0.359	1280	0.0500	0.279	0.044	131	0.488	0.050	0.493	0.51
5	19.7	0.288	1224	0.0625	0.223	0.035	105	0.607	0.040	0.408	0.33

$$m_2 = -\frac{(t_i - t_0 + a - b)r_1 e^{r_2 H} + (k\pi/Gc)(a - \Delta t_N)(r_1/r_2)}{r_1 e^{r_1 H} - r_2 e^{r_2 H}}; \quad (13)$$

$$n_2 = \frac{(t_i - t_0 + a - b)r_2 e^{r_1 H} + (k\pi/Gc)(a - \Delta t_N)(r_2/r_1)}{r_1 e^{r_1 H} - r_2 e^{r_2 H}}; \quad (14)$$

$$r_1, r_2 = \frac{\pi}{Gc}\left(\frac{k_\tau D}{2} \pm \sqrt{\frac{k_\tau^2 D^2}{4} + k_\tau D k}\right); \quad (15)$$

$$a = \frac{Gc}{k\pi}\left(\sigma - \frac{i_1}{c}\right); \quad (16)$$

$$b = \frac{G(i_1 + i_2)}{k_\tau \pi D}, \quad (17)$$

where t_i is the initial temperature of the drilling fluid, °C; H is the final depth of the borehole, m; k is the specific heat transfer coefficient, W (m °C)$^{-1}$; G is the mass flow rate of the drilling fluid, kg s^{-1}; c is the mass-specific heat of the drilling fluid, J (kg °C)$^{-1}$; Δt_N is the temperature gain at the bottom of the hole, °C; k_τ is the coefficient of nonstationary (time-dependent) heat transfer between the drilling fluid and the ice masses, W (m^2 °C)$^{-1}$; and i_1 and i_2 are hydraulic slopes in the downward and upward flows.

The specific heat transfer coefficient that accounts for the heat transfer through the hosepipe is calculated according to the following equation:

$$k = \frac{1}{(1/\alpha_1 d_1) + (1/2\lambda_h)\ln(d/d_1) + (1/\alpha d)}, \quad (18)$$

where α and α_1 are heat-conductivity coefficients in the annulus and hosepipe, W (m^2 °C)$^{-1}$; d and d_1 are the outer and inner diameters of the hosepipe, m; and λ_h is the thermal conductivity of the hosepipe material, W (m °C)$^{-1}$.

It is recommended to estimate the heat-conductivity coefficients for simple (Newtonian) fluids using the following equation:

$$\alpha, \alpha_1 = 0.021 Re^{0.8} Pr^{0.43} \frac{\lambda}{D_h}, \quad (19)$$

where Pr is the Prandtl number and λ is the thermal conductivity of the drilling fluid, W (m °C)$^{-1}$.

The Prandtl number is a dimensionless ratio defined as

$$Pr = \frac{\nu}{\beta}, \quad (20)$$

where β is the thermal diffusivity of the drilling fluid, m^2 s^{-1}.

The mass flow rate of the drilling fluid is

$$G = Q\rho_f. \quad (21)$$

The temperature gain at the bottom of the hole can be estimated according to

$$\Delta t_N = \frac{k_N N}{Gc}, \quad (22)$$

where N is the power consumed in cutting the ice by the drill head, W; and k_N is the coefficient accounting for the efficiency of the downhole driven motor, transmission and other heat sources.

Mellor and Sellman (1976) suggested to estimate the power required for cutting the ice using the specific energy E_S (N m^{-2}), which is the energy consumed per unit volume of cutting

$$N = \frac{\pi}{4} E_s (D^2 - D_i^2)\mathrm{ROP}. \quad (23)$$

Kudryashov and Yakovlev (1983) proposed to calculate the coefficient of nonstationary heat transfer between the drilling fluid and the ice masses using the following equation:

$$k_\tau = \frac{\lambda_{ice}^{0.75}}{(0.5D)^{0.25}}\left(\frac{c_{ice}\rho_{ice}}{\tau}\right)^{0.25}, \quad (24)$$

where λ_{ice}, c_{ice}, and ρ_{ice} are thermal conductivity [W (m °C)$^{-1}$], mass-specific heat [J (kg °C)$^{-1}$] and density [kg m^{-3}] of the ice masses; and τ is the circulation time, s.

The circulation time includes the time of downward flow and the time to reach the surface in the upward flow

$$\tau = \frac{H}{U_1} + \frac{H}{U_2}. \quad (25)$$

The hydraulic slopes in the downward and upward flows are calculated as follows:

$$i_1 = \frac{p_1}{g\rho_f H}; \quad (26)$$

$$i_2 = \frac{p_2}{g\rho_{f+ice} H}, \quad (27)$$

where ρ_{f+ice} is the drilling fluid density of the upward flow accounting for the density of the ice chips, kg m^{-3}.

Figure 3 shows the predicted results of the temperature distribution in the downward flow (t_1) and upward flow (t_2) for the following parameters: H = 3000 m (total length of the hosepipe 3500 m); λ_{ice} = 2.49 W (m °C)$^{-1}$; c_{ice} = 3240 J (kg °C)$^{-1}$; ρ_{ice} = 923 kg m^{-3}; E_S = 3.4 MN m^{-2}; c = 1900 J (kg °C)$^{-1}$; β = 0.1 mm^2 s^{-1}; λ = 0.12 W (m °C)$^{-1}$; λ_h = 0.4 W (m °C)$^{-1}$; t_i = −30 °C; and t_0 = −54.5 °C. The temperature of the ice and the temperature gradient were estimated according to in situ data obtained during

https://doi.org/10.1017/aog.2020.79 Published online by Cambridge University Press

the EPICA Dome C drilling project (L. Augustin, personal communication, 2011)

$$t_{\text{ice}} = -54.442 + 4.92 \times 10^{-3}h + 4.811 \times 10^{-6}h^2 - 0.4164 \times 10^{-9}h^3; \quad (28)$$

$$\sigma = 0.0043 + 1.01 \times 10^{-5}h - 1.4 \times 10^{-9}h^2. \quad (29)$$

The temperature of the drilling fluid in the hosepipe decreases due to the heat exchange with the upward cold flow, down to a minimal temperature of −48.5 °C calculated at a depth of 500 m, where it then raises. Deeper than 2600 m, the drilling fluid temperature becomes positive. When the drilling fluid reaches the drill bit, its temperature is 7.1 °C. The positive temperature in the upward flow can adversely affect the borehole wall by melting it. In the upper part of the borehole, the temperature of the drilling fluid decreases due to cooling via the surrounding ice. If the upward flow supplies melted water, this water would eventually freeze and could cause problems. This phenomenon should be taken into consideration in the test drilling operations. When the drilling fluid is back at the surface, its temperature reaches −41.1 °C. In comparison, the temperature distribution of the ice masses is also shown in Fig. 3.

The density and viscosity of the drilling fluid (Type BM3 silicone oil) vary with temperature according to Triest and Alemany (2014)

$$\rho_{\text{f}} = -0.93t + 911.3; \quad (30)$$

$$\lg(\nu + 1) = \frac{476.6}{273.1 + t} - 0.925. \quad (31)$$

These equations are applied without taking the compressibility of the drilling fluid into account. However, in the first approximation, we can use these parameters to predict the density and viscosity distribution in the downward and upward flows (Fig. 4).

The roughness coefficient, Reynolds number and pressure losses were then calculated again for the 1.25 in hosepipe with a flow rate of 32.8 L min^{-1}. The resulting pressure losses in the downward flow are higher than the previously estimated losses for the average borehole temperature (0.456 MPa vs 0.372 MPa); however, surprisingly, the recalculated pressure losses in the upward flow are lower than the previously estimated losses (0.025 MPa vs 0.067 MPa). As a result, the required outlet pressure of the pump did not change much (0.691 MPa vs 0.636 MPa).

6. Chip velocity due to drag force

In order to reduce the risk to get the probe stuck in the ice due to ice chip agglomeration, we decided to reduce the ice chip concentration as much as possible and thus, to obtain the highest possible fluid flow rate, while taking into account the energy consumption of a high—pressure pump and the resulting logistical constraints, in order to obtain the highest possible upward velocity for the ice chips.

In the following section, we determine the interaction between the drilling fluid velocity and ice chip velocity in the annulus section between the borehole sides and the hosepipe. This relationship helps to determine the minimum fluid velocity (and consequently the fluid flow rate) required to get sufficient upward motion for the ice chips.

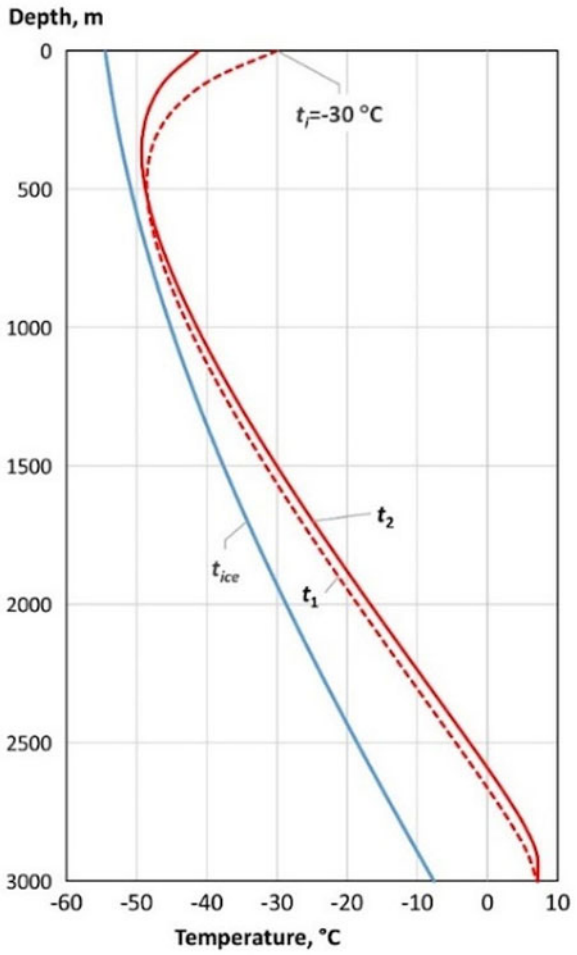


Fig. 3. Temperature distribution in the downward flow (t_1) and upward flow (t_2) of the drilling fluid; t_{ice} is the temperature distribution of the ice masses at Dome C, Antarctica.

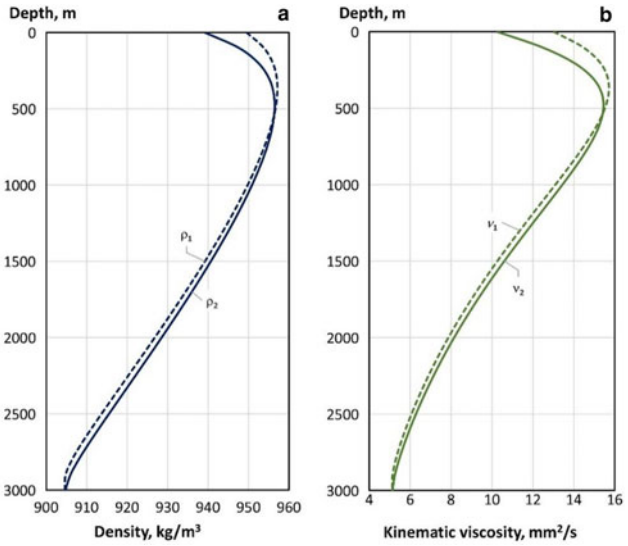


Fig. 4. Distribution of the drilling fluid density (a) and viscosity (b) in the 3000-m deep borehole.

6.1 Model simplification

Calculations were conducted for the case of BlueStar 47V3 silicone oil. Its density (ρ_{fluid}) is higher than the ice density (ρ_{ice})

https://doi.org/10.1017/aog.2020.79 Published online by Cambridge University Press

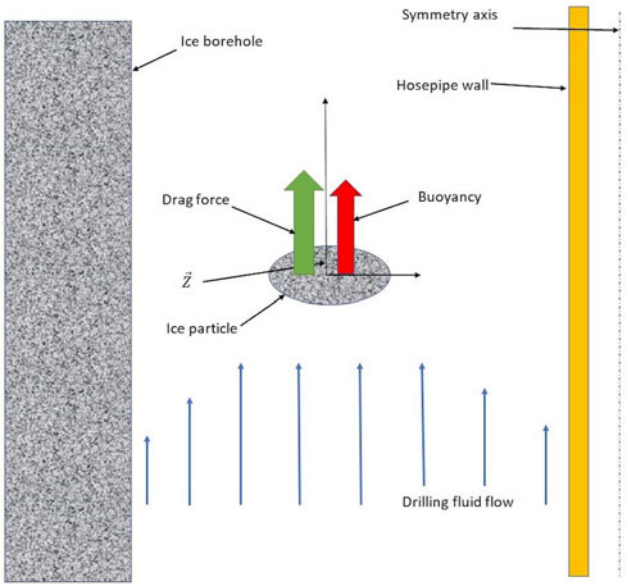


Fig. 5. Schematic of the forces applied to the ice particle on entering the fluid flow.

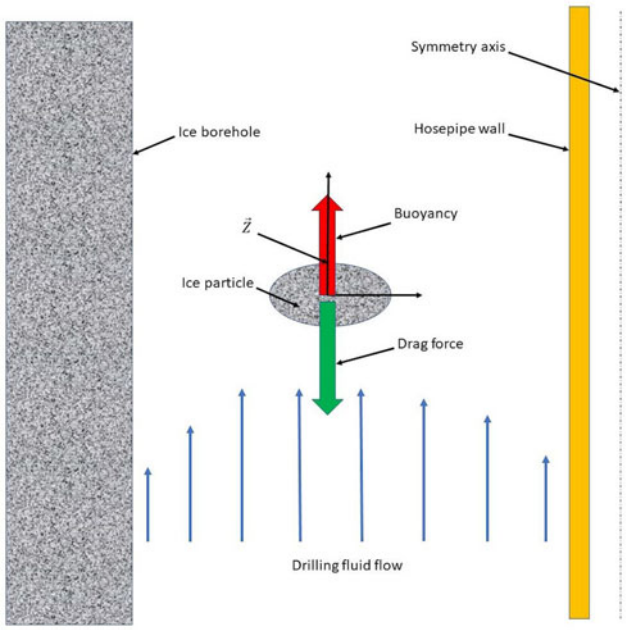


Fig. 6. Schematic of the forces on the ice particle in a state of equilibrium.

at a temperature below −20 °C. At these temperatures, the natural tendency for ice chips lying in such a fluid would thus be to come up to the surface. Inversely, the oil density is lower than the ice density at temperatures >−20 °C. At these temperatures, the natural tendency for chips is to sink in the fluid.

Taking into account the behaviour of ice chip in silicone oil, all calculations were performed considering a two-phase flow with ice chips in motion inside a fluid having its own flow rate. The ice chip concentration (<5%) is low enough to assume that there is no interaction between the ice particles and thus that ice chip motion is only due to the drag force ($\vec{F}_{\mathrm{d}}$) exerted by the fluid flow and the particles' relative weight ($\vec{P}$).

We considered two scenarios:

Scenario 1: temperature <−20 °C. The oil density is higher than the ice particle density, where the natural tendency of ice chips in oil is to move upward.

After being produced by the drill head, the ice chips accelerate in the fluid flow (with a velocity that is null just after being produced) under the combined action of two forces: drag force and relative weight. At that moment, both forces have the same direction (Fig. 5), thus accelerating the upward particle motion.

The magnitude of the drag force will decrease while the particle velocity increases (e.g. Saulnier, 2006):

$$\vec{F}_{\mathrm{D}} = \frac{1}{2} \times \rho_{\mathrm{fluid}} \times C_{\mathrm{d}} \times S_{\mathrm{part}} \times (\vec{U}_{\mathrm{fluid}} - \vec{U}_{\mathrm{part}}) \times \vec{U}_{\mathrm{fluid}} - \vec{U}_{\mathrm{part}}, \quad (32)$$

where ρ_{fluid} represents the drilling fluid density (in kg m^{-3}), S_{part} is the ice particle surface (in m^2) perpendicular to the flow, U_{part} and U_{fluid} are the ice velocity and drilling fluid velocity (in m s^{-1}), and C_{d} is the drag coefficient.

When the ice particle velocity becomes higher than the fluid flow velocity, the term ($\vec{U}_{\mathrm{fluid}} - \vec{U}_{\mathrm{part}}$) becomes negative, and the direction of the drag force is no longer upward but downward. The drag force will then slowdown the particle velocity. At one point, the drag force becomes the exact opposite of the buoyancy, and the ice particle reaches its speed limit in the equilibrium of forces (Fig. 6).

We assumed that particles are far enough from the borehole walls and from the hosepipe to consider that they are moving essentially in the central part of the annulus section and are only slightly affected by the boundary layers.

The trajectory of a particle which moves upward due to a fluid flow is usually not straight but instead follows a helical trajectory. However it has been observed (Fernandez, 2005) that for particles which have a density very close to the fluid density and for low Reynolds numbers ($Re < 100$), the particles' trajectory is nearly straight after a short transitory motion. In a first approximation, all calculations in this study were conducted in two dimensions (Fig. 6), considering a purely vertical fluid flow (along the $\vec{z}$-axis).

Scenario 2: temperature >−20 °C. In this case, the oil density is lower than the ice particle density. The natural tendency of ice chips in silicone oil at these temperatures is to move downward. The only way to get an upward motion in this situation is to generate a fluid flow creating a drag force which will compensate for the relative weight of the particle.

6.2 Fluid velocity expression

Taking these simplifications into account, the only forces that are applied to the ice particles are the particles' relative weight ($\vec{P}$) and the drag force $\vec{F}_{\mathrm{D}}$ (due to the fluid flow action on the particle).

Following Newton's laws of motion ($\sum \vec{F} = m\vec{\gamma}$) and considering that the ice particles have a steady motion without acceleration and that all the forces are applied to the particle's gravity centre (which implies that the hydraulic action of the fluid flow does not induce rotation of the particle), it is possible to write

$$\vec{P} + \vec{F}_{\mathrm{D}} = m\vec{\gamma} = \vec{0}. \quad (33)$$

Therefore

$$\vec{P} = -\vec{F}_{\mathrm{D}}, \quad (34)$$

where $\vec{P} = -(\rho_{\mathrm{ice}} - \rho_{\mathrm{fluid}}) V_{\mathrm{ice}}\, g\, \vec{z}$ is the buoyancy (the relative weight) of the ice particle in suspension in drilling fluid (e.g. Comolet, 2006) and $\vec{F}_{\mathrm{D}} = \frac{1}{2}\rho_{\mathrm{fluid}} C_{\mathrm{d}} S_{\mathrm{part}} (\vec{U}_{\mathrm{fluid}} - \vec{U}_{\mathrm{part}}) \vec{U}_{\mathrm{fluid}} - \vec{U}_{\mathrm{part}}$ is the drag force, at equilibrium, applied to the ice particle (e.g. Saulnier, 2006). In these expressions, ρ_{ice} and ρ_{fluid} represent the ice and drilling fluid density (in kg m^{-3}), V_{ice} is the ice particle volume (in m^3), S_{part} is the ice particle surface (in m^2) perpendicular to

https://doi.org/10.1017/aog.2020.79 Published online by Cambridge University Press

the flow, U_{part} and U_{fluid} are the ice and drilling fluid velocity (m s^{-1}), and C_d is the drag coefficient of the particle.

In both scenarios (temperature higher or lower than −20 °C), at equilibrium, the drag force is opposite to the relative weight of the particle and is directed downward.

Projecting Eqn (33) on the $\vec{z}$-axis gives

$$-(\rho_{ice}-\rho_{fluid})V_{ice}g+\frac{1}{2}\rho_{fluid}C_dS_{part}(U_{fluid}-U_{part})U_{fluid}-U_{part}=0. \quad (35)$$

Here again, we obtain two scenarios:

First scenario: the temperature is >−20 °C. In this case, the ice density is higher than the fluid density, the relative weight is directed downward and thus the drag force is directed upward

$$(\rho_{ice}-\rho_{fluid})V_{ice}g=\frac{1}{2}\rho_{fluid}C_dS_{part}(U_{fluid}-U_{part})U_{fluid}-U_{part}. \quad (36)$$

When the drag force is directed upward

$$U_{fluid}-U_{part}=(U_{fluid}-U_{part}). \quad (37)$$

So

$$(\rho_{ice}-\rho_{fluid})V_{ice}g=\frac{1}{2}\rho_{fluid}C_dS_{part}(U_{fluid}-U_{part})^2, \quad (38)$$

$$\Delta U=U_{fluid}-U_{part}=\sqrt{\frac{2gV_{ice}(\rho_{ice}-\rho_{fluid})}{C_d\rho_{ice}S_{part}}}. \quad (39)$$

Second scenario: the temperature is <−20 °C. In this case, the ice density is lower than the fluid density, the relative weight is directed upward and the drag force is directed downward

$$(\rho_{ice}-\rho_{fluid})V_{ice}g=\frac{1}{2}\rho_{fluid}C_dS_{part}(U_{fluid}-U_{part})U_{fluid}-U_{part}. \quad (40)$$

When the drag force is directed downward, the particle velocity is higher than the fluid velocity

$$U_{fluid}-U_{part}=-(U_{fluid}-U_{part}), \quad (41)$$

$$(\rho_{ice}-\rho_{fluid})V_{ice}g=-\frac{1}{2}\rho_{fluid}C_dS_{part}(U_{fluid}-U_{part})^2, \quad (42)$$

$$(\rho_{fluid}-\rho_{ice})V_{ice}g=\frac{1}{2}\rho_{fluid}C_dS_{part}(U_{fluid}-U_{part})^2, \quad (43)$$

$$\Delta U=U_{fluid}-U_{part}=\sqrt{\frac{2gV_{ice}(\rho_{fluid}-\rho_{ice})}{C_d\rho_{ice}S_{part}}}. \quad (44)$$

We thus obtain a relationship between the fluid velocity (U_{fluid}), the particle velocity (U_{part}) and the drag coefficient (C_d). According to the literature on fluid mechanics, the drag coefficient depends on the particle's Reynolds number (Re_{part}), which itself depends on the fluid and particle velocity and on the fluid viscosity (ν_{fluid} is the kinematic fluid viscosity in $m^2\,s^{-1}$)

$$Re_{part}=\frac{d\vec{U}_{fluid}-\vec{U}_{part}}{\nu_{fluid}}=\frac{d\,(U_{part}-U_{fluid})}{\nu_{fluid}}. \quad (45)$$

Without simplification, it is not possible to obtain the fluid velocity as a function of the particle velocity in a simple manner.

Considering the borehole geometry (diameter ≈ 120 mm), the hosepipe OD = 44 mm, and the limitations on fluid flow (fluid flow should be <60 L min^{-1} in order to minimise the pump requirement and thus logistic costs), the fluid velocity in the annulus section (between the borehole wall and hosepipe) must be <0.1 m s^{-1}.

A target fluid velocity range was chosen. This velocity range arises from the compromise of having the highest possible particle velocity and with the lowest logistical costs. Three different fluid velocities were chosen: 0.05, 0.07 and 0.1 m s^{-1}. Considering this fluid velocity as an input to Eqn (44), the remaining unknown required to calculate the fluid velocity is the drag coefficient of ice chips.

6.3 Ice chip drag coefficient estimation

Different expressions are available to calculate C_d (e.g. Schiller and Nauman, 1935) depending on the shape of the particle and on the Reynolds number. Table 3 shows some of the relationships for spherical particles or discs.

We compared these relationships with experimental results. In order to simplify the latter, tests were carried out at ambient temperature (~20 °C), which is acceptable because C_d does not depend on temperature. Here, ice chips were considered to be small rectangular sheets (length = 3 mm, width = 1 mm and high = 0.5 mm). The experiments were carried out to determine the drag coefficient of small particles of this size. Small polyethylene high density (HDPE) plastic particles with a density of 950 kg m^{-3} having nearly the same shape as ice chips were dropped in a long vertical channel containing immobile water or silicone oil (both tests were performed). The time needed by the particle to travel between two points was measured far enough from the surface in order to be sure that they had reached their maximal falling speed. The particle velocity is measured (and constant) and the fluid velocity is known (U_{fluid} = 0 m s^{-1} as the fluid in the experimental channel is static), and the only unknown parameter in Eqn (44) is the drag coefficient C_d

$$C_d=\frac{2gV_{Ice}(\rho_{fluid}-\rho_{part})}{(\rho_{fluid}S_{ice}U_{ice}^2)}. \quad (46)$$

With

$$Re_p=\frac{dU_{part}}{\nu_{fluid}}. \quad (47)$$

The free-falling particle velocity was measured for three different ranges of particle sizes (blue, green and red dots in Fig. 7). This graph gives the drag coefficient of small rectangular particles as a function of Reynolds numbers <50. At very low Reynolds numbers, the uncertainty is too high and the results cannot be trusted because it was not possible to get repeatable measurements due to the low particle speeds and the resulting erratic particle trajectories. The range of Reynolds numbers where the experiment results are meaningful and comparable with the literature for such particle sizes is between 25 and 50 Re_{part}.

https://doi.org/10.1017/aog.2020.79 Published online by Cambridge University Press

Table 3. Drag coefficient for a sphere and disc

Nature of the flow	Range of particle's Reynolds number	Expression of the drag coefficient for a sphere	Expression of the drag coefficient for a disc
Stokes flow	$10^{-4} < Re_{part} < 1$	$\frac{24}{Re_p}$	$\frac{64}{\pi Re_p}$
Allen-Cahn flow (intermediate flow)	$1 < Re_{part} < 10^3$	$\frac{18.5}{Re_{part}^{0.6}}$	$\frac{64}{\pi Re_{part}}(1 + 0.138\, Re_p^{0.792})$
Newtonian flow (turbulent flow)	$10^3 < Re_{part} < 5 \times 10^5$	0.44	1.14

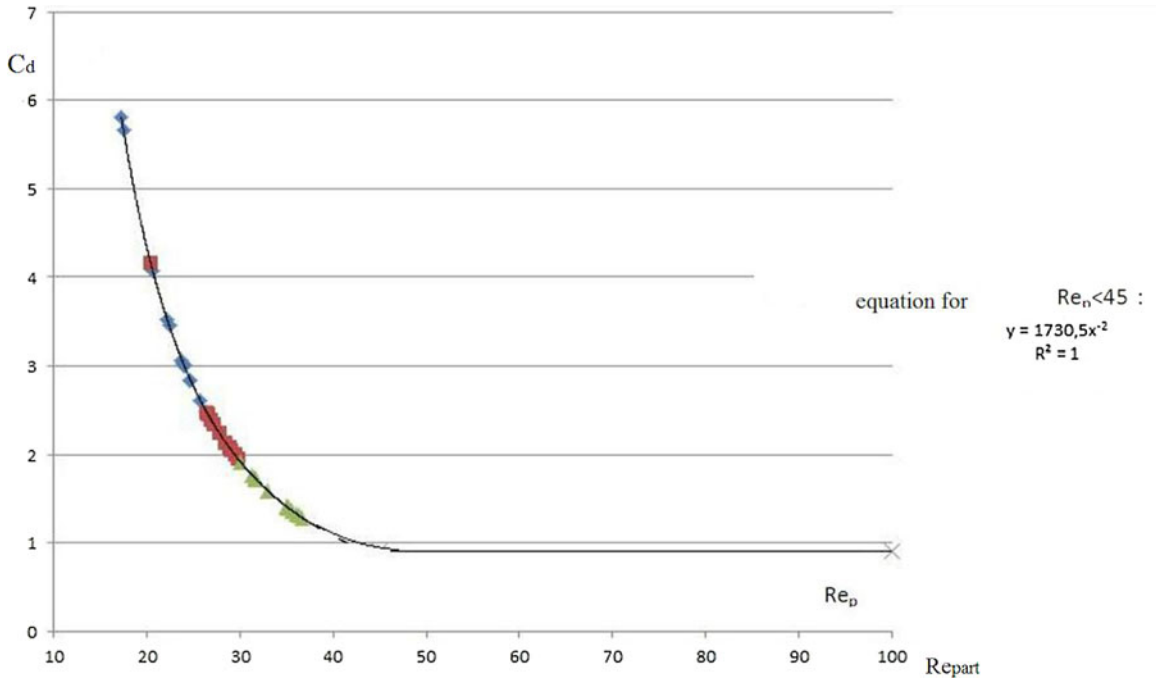


Fig. 7. Drag force coefficient for plastic particles with the same shape as ice chips (x: Reynolds number and y: Drag coefficient).

In this range of values, it is possible to use the expression (Wingert, 2012):

$$C_d = 1730.5\, Re_{part}^{-2} \quad \text{for } 20 < Re_{part} < 50, \tag{48}$$

$$C_d \approx 1 \quad \text{for } Re_{part} > 50. \tag{49}$$

6.4 Calculation of the fluid velocity required to obtain the target particle velocity

At this point:

- Three potential fluid velocities have been chosen (0.05, 0.07 and 0.1 m s^{-1}).
- The drag coefficient of ice chips can be calculated as a function of fluid velocity. Unfortunately in the range of fluid velocities, we planned to use, the particular Reynolds number is too low to use the relationship established by Wingert for ice particles. Therefore, as a first approximation, we calculated the drag coefficient by considering ice chips as small discs (Table 3).
- The velocity difference ΔU ($U_{part} - U_{fluid}$) was calculated in two different ways. First, by making iterations on the particle velocity and thus directly calculating $\Delta U = (U_{part} - U_{fluid})$. Second, by using Eqn (39) and again making iterations on U_{part}. At each iteration, the two values of ΔU are compared. When the relative error between these two calculated ΔU values is <10%, we considered that the particle velocity corresponds to the chosen fluid velocity (Table 4).

Based on this calculation, if the fluid velocity in the annulus section between the hosepipe and the borehole is 0.05 m s^{-1}, then the ice particle velocity will be 0.054 m s^{-1}.

6.5 Conclusions of these calculations

In the range of fluid velocities considered (between 0.05 and 0.1 m s^{-1}), the upward particle velocity and the upward drilling fluid velocity in the annulus section between the borehole walls and the hosepipe are of comparable magnitude.

For our drilling application, the drilling fluid upward velocity is usually relatively low and thus the ice chip velocity (during ice chip transport) is close to the fluid velocity. If the fluid is heavier than the ice, the upward velocity of the ice particle will be slightly higher than the fluid velocity, and vice versa, if the fluid is lighter than the ice, the upward velocity of the ice particle will be slightly lower than the fluid velocity.

In this range of speeds, the relationship that was established to calculate the drag coefficient for ice chips is not applicable. However, it is still possible to use the drag coefficient of a small disc in the drag force and fluid velocity calculations.

Obviously, these calculations need to be confirmed by experimental measurements under real conditions.

7. Experimental tests

7.1 Tests in a cold room

To confirm these results, a testing bench was set up in the cold rooms of the laboratory (Fig. 8). A hydraulic pump generates a

https://doi.org/10.1017/aog.2020.79 Published online by Cambridge University Press

Table 4. Particle velocity calculation as a function of fluid velocity in the annulus section (at negative temperatures >−20 °C)

Fluid velocity, m s^{-1}	Particle velocity calculated, m s^{-1}	Re_{part}	C_d (disc correlation)	ΔU calculation from (39), m s^{-1}	Direct ΔU calculation, m s^{-1}	Relative error, %
0.05	0.054	0.61	36	0.0037	0.004	7.5
0.07	0.074	0.55	40	0.0036	0.004	10
0.1	0.1045	0.60	36	0.0039	0.004	2.5



Fig. 8. Photo of the test setup in the cold room.

fluid flow through pipes with one part of the circuit being made with a transparent material in order to visualise the fluid flow. The whole circuit was filled with silicone oil BM3 (20 l) and ice chips (1 l). The goal of this setup was to confirm the upward ice chip velocity depending on the fluid flow rate. In the transparent pipe section, the pipe ID is 50 mm, therefore, as we know the pump flow rate (from a flow meter in this part of the circuit), it is possible to obtain the mean fluid velocity in this section:

$$U_{\text{fluid}} = \frac{Q}{S}. \tag{50}$$

Many pumps were tested before finding a suitable one. Some of the pumps with plastic impellers were destroyed, as silicone oil moved through the plastic impellers due to its very low surface tension, generating cavitation behind the impellers. Others with very thin channels generated ice chips agglomeration in the rotor. Finally, a pump which is usually used in cold room machinery was successfully set up. The nominal flow rate of these pumps is close to 80 L min^{-1} which results in a 0.68 m s^{-1} fluid velocity in the vertical pipe. This is much higher than what is needed to be tested. Therefore, a frequency converter was set up to drive the pump at a lower frequency and thus to generate much lower flow rates. The lowest frequency that could be imposed on the pump motor was 16 Hz (60 Hz being the nominal frequency of the pump motor), which resulted in a 20 L min^{-1} flow rate and thus a 0.17 m s^{-1} fluid and ice chip upward velocity. This is still higher than the fluid velocity required for the SUBGLACIOR project. With a flow rate close to 20 L min^{-1}, we observed a very thin layer of ice chips sticking to the pipe walls after 24 h of testing, and a small deposit of ice chips just in front of the flow meter. These layers were not compact and disappeared immediately after increasing the flow rate back up to 60 L min^{-1}. At a low flow rate, we generate a lot of hydraulic perturbations and a recirculation area close to the flow meter (variable area flow meter with a conical plastic flow indicator).

The same test was conducted at 20 L min^{-1} (0.17 m s^{-1}) and without the flow meter. Apart from a tiny deposit of ice chips on the pipe walls, no special conglomeration of ice chips was observed after a 96 h test.

Despite the difficulty to test this chip's behaviour in the fluid circulation loop in the cold room, we have been able to conclude that:

- Ice chips move vertically together with the upward fluid flow. Sometimes their trajectories become erratic but they never move downward.
- No significant ice chip agglomeration was noticed.

7.2 Field tests

The whole SUBGLACIOR drilling probe setup was tested at Concordia Station in Antarctica during the field campaign 2016–17, including the fluid flow loop (pump, hosepipe and probe) over a few hours of continuous operation (Fig. 9).

This allowed us to verify that the fluid flow circulation was efficient in real conditions of the Antarctic plateau. The pump was run at various flow rates, between 20 and 35 L min^{-1}. Within this range, a suitable and continuous fluid flow was obtained between the probe head and the surface, carrying ice chips (and HDPE chips produced from the casing) when drilling. The pressure measured was in the range of what had been calculated in Section 4 (Table 5).

However, the measured pressure was not stable, and we did not run the pump for long enough to be able to prove the pressure requirement over a long-term period. Still, we could conclude that the real pump pressure requirement is of the same order of magnitude as resulting from our calculations in Section 4.

8. Conclusions

Efficient ice chip recovery is a critical aspect of most deep ice drilling operations. It is particularly acute for the SUBGLACIOR project where probe penetration through the ice sheet must ideally take place in a single run. Ice chip transport in the borehole is achieved by the circulation of drilling fluid. Hence, selecting the pump that will generate the fluid flow and determining the hydraulic working conditions (flow rate, pressure drop and power consumption) is of high importance.

https://doi.org/10.1017/aog.2020.79 Published online by Cambridge University Press

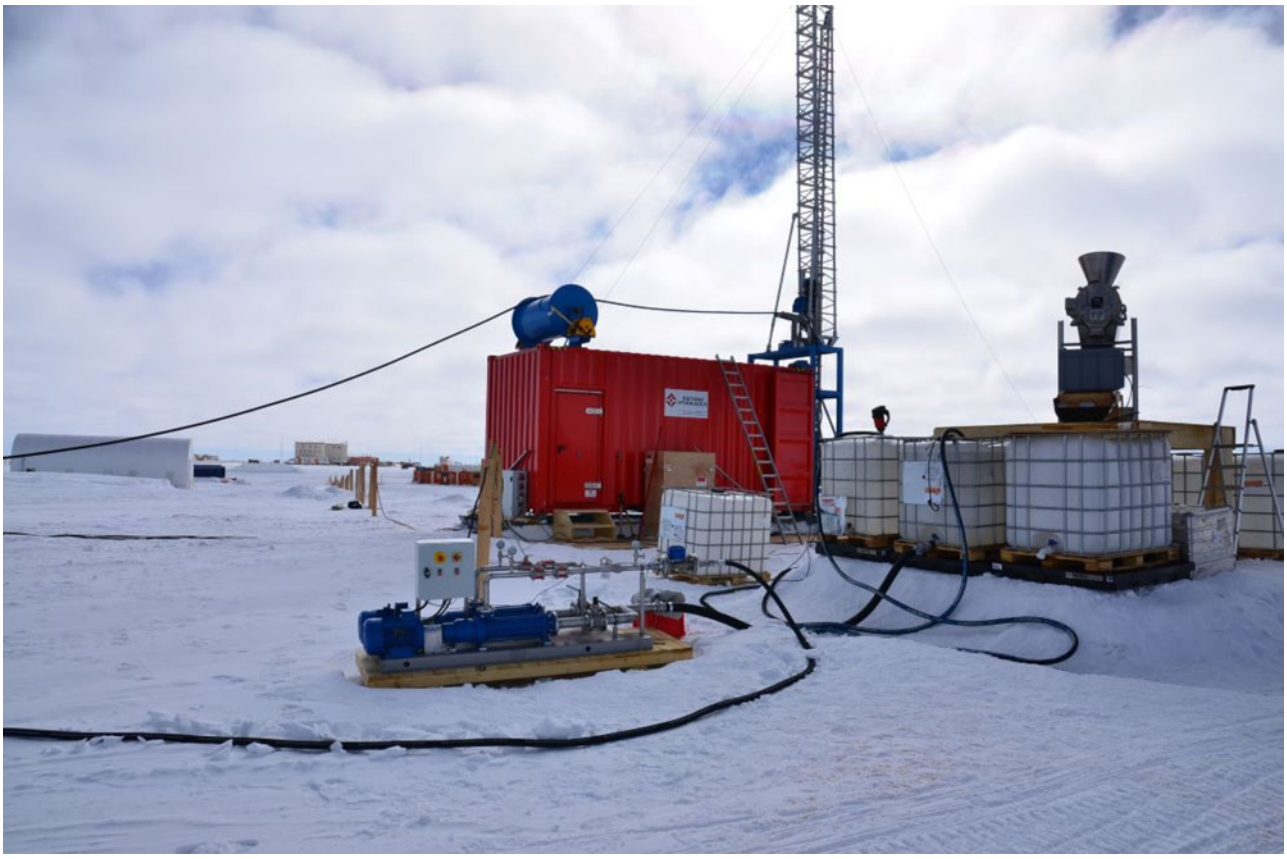


Fig. 9. The SUBGLACIOR surface high-pressure pump (1), with the drilling fluid containers (2), the fluid and chips separation device (3 – on the top of IBC drilling fluid containers) and the hydraulic hosepipe on the top of the red container (4).

Table 5. calculated and measured pump pressure drop

Flow rate, L min^{-1}	Calculated pressure, MPa	Mean measured pump pressure, MPa
20	0.713	0.7.1
25	0.875	0.78
30	1.6	1.2

Through this study, we quantitatively demonstrate that the ice chip velocity in the case of ice drilling is nearly equal to the fluid velocity. Prior to this study, this result was merely an empirical assumption. Our calculations show that in the case of the SUBGLACIOR project where ice chips are transported along a very long stream line, the fluid velocity should be as large as possible. On the other hand, head losses and power consumption increase significantly with the flow rate. We thus determined an optimal compromise between hydraulic requirements for efficient chip entrainment, pump requirements and logistic constraints. The results from our calculations are of the same order of magnitude as the obtained experimental and Antarctic field test results, and they could thus be used in other drilling projects in order to size the hydraulic drilling fluid loop.

Theoretical estimations of drilling fluid temperature distribution in the borehole showed that due to the heat exchange between downward flow, upward flow and surrounding ice and thermal influence of hydraulic friction, the drilling fluid is warmed up in the lowest part of the borehole, up to positive temperatures. The positive temperature in the upward flow can adversely affect the borehole wall by melting them. This possible phenomenon should be accounted for in the drilling process design.

Acknowledgements. The research leading to these results has received funding from the European Community's Seventh Framework Programme ERC2011 under grant agreement no. 291062 (ERC Ice & Lasers) and from the French Agence Nationale de la Recherche (ANR) under grant agreement no. SIM15-6-ANR-11-BS56-0019 (ANR SUBGLACIOR). This project was conducted thanks to the technical support of the French Drilling and Coring Facility (C2FN – Ice). Additional funding support was provided by the BNP Paribas Foundation as well as 'Equipement d'Excellence' EquipEX CLIMCOR (ANR-11-EQPX-0009-CLIMCOR). Fieldwork was supported by IPEV (France, through the 'SUBGLACIOR' project no. 1119) and PNRA (Italy) at Concordia Station.

References

Alemany O and Mityar H (2007) Viscosity and density of a two phase drilling fluid. *Annals of Glaciology* **47**, 141–146.

Alemany O and 21 others (2014) The SUBGLACIOR drilling probe: concept and design. *Annals of Glaciology* **55**(68), 233–242.

Belvins DR (1984) *Applied Fluid Dynamics Handbook*. Belvins: KRIEGER, pp. 41–87.

Brater EF, King HW, Lindell JE and Wei CY (1996) *Handbook of Hydraulics*, 7th Edn. New York: McGraw-Hill.

Comolet R. (2006) Mécanique experimentale des fluides, vol. **2**, pp. 228–264

Fernandez PC (2005) Étude expérimentale de la dynamique de corps mobiles en ascension dans un fluide peu visqueux. *Thèse de l'Ecole Polytechnique de Toulouse*.

Kudryashov BB and Yakovlev AM (1983) Burenie skvazhin v merzlikh porodakh [drilling in permafrost], Moscow. *Nedra* **286**, pp. (in Russian).

Mellor M and Sellman PV (1976) General consideration for drill system design. *Proc. of the Symp. in Ice-Core Drilling, 28–30 August 1974*. Lincoln, USA: University of Nebraska, Lincoln: University of Nebraska Press, pp. 77–111.

Mikhailova ND (1985) *Tekhnicheskoe Proektirovanie Kolonkovogo Burenia [Technical Design of Core Drilling]*. Moscow: *Nedra* 200, pp. (in Russian).

https://doi.org/10.1017/aog.2020.79 Published online by Cambridge University Press

Nguyen JP (1993) *Techniques D'exploitation Pétrolière, Le forage*. (Éditions Technip).

Saulnier C (2006) *Modélisation Numérique Tridimentionnelle de L'écoulement Réactif Triphasique Gaz-Goutte Particule au Sein d'un Réacteur à lit Fluidisé*. (PhD thesis, INP Grenoble).

Schiller L and Nauman A (1935) A drag coefficient correlation. *VDI Zeitung* **77**, 318–320.

Talalay PG (2006) Removal of cuttings in deep ice electromechanical drills. *Cold Regions Science and Technology* **44**, 87–98.

Talalay PG and Gundestrup NS (2002*a*) Hydrostatic pressure and fluid density profile in deep ice bore-hole. *Memoirs of National Institute of Polar Research* **56**, 171–180.

Talalay PG and Gundestrup NS (2002*b*) Hole fluids for deep ice core drilling. *Memoirs of National Institute of Polar Research* **56**, 148–170.

Triest J and Alemany O (2014) Drill fluid selection for the SUBGLACIOR probe: a review of silicon oil as a drill fluid. *Annals of Glaciology* **55**(68), 311–321.

Wingert L (2012) *SUBGLACIOR Hydraulic Consideration*. (Master's essay, Grenoble University).

https://doi.org/10.1017/aog.2020.79 Published online by Cambridge University Press